JCTC Journal of Chemical Theory and Computation

ARTICLE

pubs.acs.org/JCTC

Theoretical Study of the Luminescent States and Electronic Spectra of UO_2Cl_2 in an Argon Matrix

Jing Su,[†] Yi-Lei Wang,[†] Fan Wei,[†] W.H.E. Schwarz,[†,‡] and Jun Li[*,†]

[†]Department of Chemistry and Laboratory of Organic Optoelectronics and Molecular Engineering of the Ministry of Education, Tsinghua University, Beijing 100084, China

ABSTRACT: The electronic absorption and emission spectra of free UO_2Cl_2 and its Ar-coordinated complexes below 27 000 cm^{-1} are investigated at the levels of ab initio complete active space second-order perturbation theory (CASPT2) and coupled-cluster singles and doubles and perturbative triples [CCSD(T)] using valence 3ζ-polarized basis sets. The influence of the argon matrix in the 12K experiment on the electronic spectra is explored by investigating the excited states of argon complexes $Ar_nUO_2Cl_2$. The calculated two most stable complexes with $n = 2, 3$ can explain the observed two matrix sites corresponding to the experimental two-component luminescence decay. In these uranyl complexes, Ar-coordination is found to have little influence on the $^3\Phi$ ($\Omega = 2_g$) character of the luminescent state and on the electronic spectral shape. The calculations yield a coherent assignment of the experimental excitation spectra that improves on previous assignments. The simulated luminescence spectral curves based on the calculated spectral parameters of UO_2Cl_2 from both CASPT2 and CCSD(T) agree well with experiment.

INTRODUCTION

The study of optical properties of uranyl (UO_2^{2+}) compounds has a long history.[1−3] Various systems exhibit related absorption and emission spectra, in particular in the low-temperature region. The fluorescence spectra are characterized by several vibrational progressions based on a common electronic origin. The intensity distribution of the fluorescence spectra changes with the ligands coordinated to the uranyl moiety. That is, the spectral shapes inform about the electronic and geometric structures of the respective uranyl complexes.

Time-resolved laser-induced fluorescence (TRLIF) has become a common tool to study the speciation of actinides (IUPAC: actinoids) in natural and artificial environments.[4] This spectroscopic technique is important for an atomistic understanding of the interactions of actinides with various inorganic and organic/biochemical ligands and provides the basic information for handling actinide contaminations in the environment and in biological systems, including the human body.[5,6] Theory-assisted reconstruction of knowledge from experimental data is nowadays possible for both weakly perturbed molecules or building groups as well as for complex condensed phases in thermodynamic equilibrium.[7]

We have recently investigated structures, stabilities, and the vibration-resolved luminescence of uranyl−glycine−water complexes in solution, applying comparatively simple theoretical strategies.[7] To improve on the level of spectral simulations, advanced correlated ab initio methods including spin−orbit (SO) coupling are required for open-shell excited states, refining simple density functional theory (DFT) which is often applicable for actinide closed-shell ground-state species. However, SO-complete active space second-order perturbation theory (CASPT2) or SO-multireference configuration interaction with single and double substitutions (MRCISD) are extremely demanding for such systems, due to the complexity of the actinide valence shell and the diversity and lack of symmetry of the coordination structures embedded in first and second solvent shells. On the other hand, many details of the experimental solution spectra are washed out, in particular concerning the rotational, vibrational, and electronic near-degenerate fine structure.

Recently, Heaven's group has reported electronic spectra of single UO_2Cl_2 molecules in a solid Ar matrix,[8] where UO_2Cl_2 has a significantly simpler coordination structure than the multitude of uranyl complexes in aqueous solution. The peaks of the fluorescence spectra remain sharp and well-separated; the assignment of different vibrational modes and low-electronic states comes into reach. Accordingly, the $Ar_n-UO_2Cl_2$ system is a promising candidate for the high-level path of theoretical calculations and spectra simulations.

The purpose of the present paper is the theoretical analysis of geometric and electronic structure and the computational simulation of luminescence of UO_2Cl_2 by using state-of-the-art quantum chemical methods. Before describing the theoretical methodology (Computational Details) and analyzing the computational results (Computational Results and Discussion), we briefly summarize the current understanding of uranyl and the state of experimental and theoretical knowledge of the uranyl chloride complexes.

Model Concepts for Uranyl Compounds. In order to understand chemical bonding, excited states, and absorption and emission spectra of uranyl and its complexes (Figure 1), we refer to the axial-symmetric molecular orbitals (MOs) of bare uranyl in Figure 2.[9] At the nonrelativistic and scalar relativistic levels of approximation, the U-5f type MOs under $D_{\infty h}$ symmetry are split into σ_u and pairs of π_u, δ_u and ϕ_u and the U-6d type MOs into σ_g and pairs of π_g and δ_g. In an ionic picture, all valence electrons are assigned to O^{2-}, and uranium obtains the oxidation state U^{VI}. The U-7s shell is energetically pushed up upon ligand coordination on

Received: June 19, 2011
Published: August 25, 2011

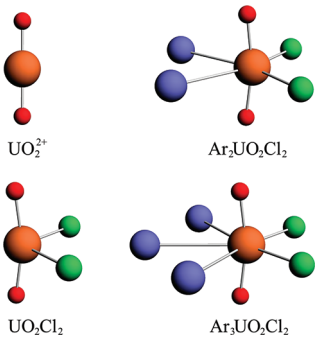

Figure 1. Geometric Structures of UO_2^{2+}, UO_2Cl_2, $Ar_2UO_2Cl_2$, and $Ar_3UO_2Cl_2$.

U(VI) and can be neglected in qualitative discussions of uranyl complexes.

The occupied 2pσ,π valence shells of the two terminal O^{2-} anions are stabilized by the U-5f,6d manifold of valence orbitals with matching symmetry. The 12 valence electrons of UO_2^{2+} participate in dative bonding through σ_g and σ_u and pairs of π_u and π_g canonical MOs, corresponding to U≡O triple bonding. Herein σ_u is the highest occupied molecular orbital (HOMO) due to a push-from-below via U-6p mixing, while the order of the slightly lower, near-degenerate σ_g, π_u, and π_g levels varies somewhat with equatorial coordination. The antibonding counterparts remain empty, see Figure 2.

In the bare uranyl dication, the U-5fδ_u, 5fϕ_u and 6dδ_g type orbitals have no symmetry-matching counterparts from the O atoms and do not participate in O−U−O bonding. These empty orbitals remain nonbonding and localized on U but are available for weaker σ and π donor interactions of Lewis bases in the equatorial plane. Thus, the ground states of the uranyl−dichloride and dichloride−argon complexes are of closed-shell type and derive from the $^1\Sigma_g^+$ state in $D_{\infty h}$ symmetry. The lowest excited states correspond to electronic transitions from U−O bonding σ_u to nonbonding U-5fϕ_u and 5fδ_u type MOs (see the arrow in Figure 2), yielding $^{1,3}\Delta_g$ and $^{1,3}\Phi_g$ states. With the inclusion of SO-coupling, $^3\Delta_g$ splits into Π_g, Δ_g, and Φ_g, ($\Omega = 1_g, 2_g, 3_g$) and $^3\Phi_g$ splits into Δ_g, Φ_g, and Γ_g. ($\Omega = 2_g, 3_g, 4_g$).

Known Uranyl Chloride Complexes. Experimentally, the absorption and fluorescence spectra of $[UO_2Cl_4]^{2-}$ in crystals have been extensively investigated by Denning and others.[10,11] Due to environmental concerns of uranyl ions released from nuclear waste, much work has been invested on the solution chemistry of uranyl complexes. Görller-Walrand et al.[12] reported that uranyl chloride complexes in various organic solvents have spectra consistent with those from crystalline materials.

Theoretical investigations of excited states of actinide compounds have been challenging. Early efforts include calculations with various DFT approximations.[2,13,14] Zhang, Matsika, and Pitzer[15,16] started the ab initio theoretical investigation of electronic excited states of UO_2^{2+} and $Cs_2UO_2Cl_4$ with the SO−CI approach. Afterward, Pierloot et al.[17] investigated $[UO_2Cl_4]^{2-}$ applying SO-CASPT2 methods, obtaining better agreement for the experimental electronic excitations and the O−U−O symmetric stretching vibration. They also performed time-dependent (TD)DFT calculations with state-averaged optimized potentials (SAOP) and SO-coupling and obtained smaller U−O bond length expansions for the excited states and a different luminescent state than with CASPT2.[18] The influence of solvent coordination in acetone on the absorption spectra of UO_2Cl_2 and $UO_2Cl_3^-$ has also been studied with the CASPT2 method.[19]

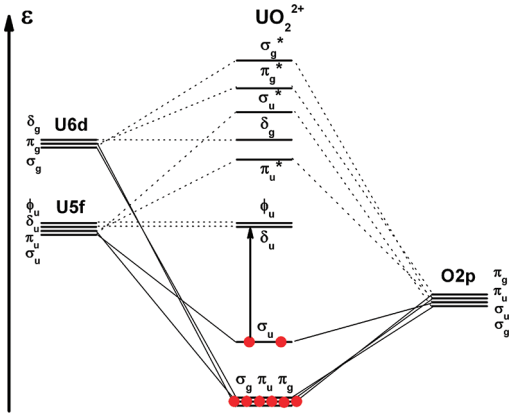

Figure 2. Qualitative scalar-relativistic valence orbital energy level schemes of U and O atoms and uranyl ($D_{\infty h}$) in the middle. The vertical arrow indicates the lowest electronic excitations.

COMPUTATIONAL DETAILS

Structures and spectra of free UO_2Cl_2 and its Ar-coordinated complexes were investigated by using CASPT2 and CCSD(T) methods, with and without SO-coupling, as implemented in the MOLPRO 2008.1 program.[20] Various $Ar_nUO_2Cl_2$ complexes were treated in a first step at the DFT level, using the ADF 2009.1 software.[21]

It has become well-known that atomic effective core potentials (ECPs) can reduce the computational expenses of self-consistent field (SCF), multiconfiguration self-consistent field (MCSCF) and CC approaches drastically. When using ECP-adapted basis sets together with ECPs, there is no loss of reliability as long as the core−valence sets are appropriately selected.[22] In addition, relativistic ECPs (RECPs) inherently account for SO-coupling which also holds for the relativistic zeroth-order regular approximation (ZORA). Therefore, we used the Stuttgart energy-consistent RECPs[23] for Cl, Ar, and U, where the $1s^22s^22p^6$ cores of Cl and Ar were treated by the scalar ECP10MWB ones, while optimizing the 3s3p valence shells, and the $1s^2-4f^{14}$ core for U was treated by the scalar and SO-coupled ECP60MWB one, with the 5spdf, 6spd, and 7sp semicore and valence shells optimized. We applied the 6-311+G* basis set for O,[24] the ECP10MWB for Cl and Ar with an additional d-polarization function (ζ=0.75) for Cl, and ECP60MWB-SEG basis set for U, respectively. The atomic core shells and the U-5spd were not correlated.

In the DFT calculations, we used the PBE functional and the scalar relativistic ZORA approach. The frozen core approximation and TZ2P bases were applied.[25]

Geometries and Vibrational Frequencies. Geometric optimizations of the electronic ground states of UO_2^{2+} in $D_{\infty h}$ and of UO_2Cl_2 in C_{2v} symmetry with CASPT2 and CCSD(T) were converged to gradients $<1.0 \times 10^{-4}$. The most stable $Ar_nUO_2Cl_2$ complexes were at first screened out for $n = 1-4$, using the ADF binding energy analysis and were then further optimized with CCSD(T) calculations. The two most stable structures were also optimized with the CASPT2 approach. Vibrational analyses were performed for the UO_2Cl_2 ground state at the CCSD(T) level.

Table 1. Correlation of Symmetry Species of Point Groups $D_{\infty h}$ and C_{2v}

$D_{\infty h}$	C_{2v}
Σ_g^+	A_1
Σ_u^+	B_1
Π_g, Δ_u, Φ_g	$A_2 + B_1$
Π_u, Δ_g, Φ_u	$A_1 + B_2$

Born−Oppenheimer (BO) potential energy curves of the SO-averaged and SO-coupled excited electronic states versus the U−O distances were at first scanned in steps of 1 pm, with the other geometric parameters fixed at their ground-state values. The expansions of the U−O distances in the excited states were obtained from polynomial interpolation. For the lowest excited luminescent state, the equilibrium values of the other geometric parameters were then similarly approximated, keeping the U−O distance of the state fixed. Thereby, the approximate U−O equilibrium distances, vertical and adiabatic excitation energies, and O−U−O symmetric stretching frequencies were determined. The error of this approximation applied to the ground state was less than 2 cm^{-1}.

Electronic States. For simplicity, we use approximate $D_{\infty h}$ symmetry notations for orbitals and states of all species, except where explicitly noted otherwise. The relations between $D_{\infty h}$ and C_{2v} (UO_2Cl_2, $Ar_{2,3}UO_2Cl_2$) symmetry species within the coordinate system used in our calculations are given in Table 1.

RASSCF/CASPT2/SO Calculations. The active spaces for ground-state CASSCF calculations of all molecular species were confined to the UO_2^{2+} moiety: The six bonding and six antibonding (*) MOs of σ_g, σ_u, π_g, and π_u type from the U-5f,6d and two O-2p shells with 12 valence electrons were correlated by CAS(12,12). The active spaces for the excited states contained in addition nonbonding U-5f type orbitals of δ_u or ϕ_u symmetry (Figure 2), giving 12 electrons in 14 orbitals for $D_{\infty h}$-UO_2^{2+}, denoted as CAS(12,14) hereafter, or 12 electrons in 13 orbitals for C_{2v}-UO_2Cl_2 and C_{2v}-$Ar_{2,3}UO_2Cl_2$, i.e., CAS(12,13). In the equatorially ligated uranyl species (Figure 1), the degeneracy of δ_u and ϕ_u is lifted, with little orbital and configuration mixing, as known from the literature.[17,26] CAS(12,16) calculations with both δ_u or ϕ_u pairs simultaneously in the active space were deemed unnecessary.

SO-averaged CASPT2 calculations were performed on the ground states and on all excited states arising from single excitations out of the σ_u HOMO into the nonbonding orbitals of U-5fδ_u,ϕ_u type, which gives four singlets and four triplets. Individually optimized CASSCF orbitals were used for each state, except for the singlet excited states of same symmetry as the ground state. Here, the ground-state orbitals helped converging to correct occupation schemes. A level shift of 0.3 au was applied to improve the CASPT2 convergence.

For UO_2^{2+}, the g_1-corrected CAS Fock-operators were also employed in order to obtain a balanced treatment of closed-shell ground and open-shell excited states. Because of the near degeneracy of some excited states of UO_2Cl_2, this was not always feasible. Therefore, the g_1-corrections of respective states of UO_2^{2+} were added to the uncorrected values of the states of UO_2Cl_2, as suggested by Pierloot (designated as g_1').[17]

SO coupling was treated by a restricted RAS-SI/SO approach[27,28] in an active space of the mentioned 16 orbitals, labeled RAS(12,16), where up to 4 electrons were excited. The SO-averaged restricted active space self-consistent field (RASSCF) singlet and triplet wave functions were determined in the basis of state averaged (SA) RASSCF orbitals of the ground and all excited singlet states. The resulting RASSCF wave functions were then used to construct a 17 × 17 SO coupling matrix, where the diagonal elements were correlation corrected by using the CASPT2 energies. Single-point SA-CAS(12,16)-SCF test calculations confirmed that the errors remain <10 cm^{-1} for UO_2^{2+} and <20 cm^{-1} for UO_2Cl_2. This combination of RASSCF/SI-SO with CASPT2 energy is labeled as RASSCF/CASPT2/SO. Calculations on UO_2^{2+}, NUO^+, UN_2, and UF_6 molecules using this approach have well reproduced the experimental data.[26,29]

Table 2. Geometric Parameters of UO_2^{2+} and UO_2Cl_2 from CASPT2 and CCSD(T) Calculations for the Ground and Four Low Excited Triplet States at the SO-Averaged Level

molecule	state in $C_{2v}(D_{\infty h})$	R_{U-O}, pm	R_{U-Cl}, pm	∠OUO, °	∠ClUCl, °
		CASPT2			
UO_2^{2+}	$(^1\Sigma_g^+)$	169.37		180.0	
UO_2Cl_2	$^1A_1(^1\Sigma_g^+)$	175.29	249.12	165.8	106.8
		CCSD(T)			
UO_2^{2+}	$(^1\Sigma_g^+)$	169.03		180.0	
UO_2Cl_2	$^1A_1(^1\Sigma_g^+)$	174.77	250.92	165.8	107.7
	$^3A_1(^3\Delta_g)$	179.73	250.19	161.8	102.8
	$^3B_2(^3\Delta_g)$	179.45	251.65	164.5	104.2
	$^3B_1(^3\Phi_g)$	181.18	251.10	158.2	101.5
	$^3A_2(^3\Phi_g)$	181.08	252.09	158.6	102.3

RASSCF/CCSD(T)/SO Calculations. The CASSCF/CCSD(T)/SO method had been shown to be quite accurate for various properties of transition-metal compounds.[30−32] We here applied such an approach to the excited states of UO_2Cl_2 and $Ar_{2,3}$-UO_2Cl_2, but constructed the SO coupling matrix from SA-RASSCF wave functions. For the ground and excited triplet state energy curves, the SO-averaged scheme was applied at first. Then the CASPT2 energy difference between the excited singlet and triplet pair was obtained pointwise to estimate the excited singlet energy curves. The SO coupling effect was included in the same way as above with the diagonal elements corrected by the CCSD(T) state energies.

Simulation of Luminescent Spectra and Normal Coordinates Analysis. Following our previous work,[7] the profiles of the luminescence spectra were modeled using the Franck−Condon formulas of Fonger and Struck.[33] In this approach vibrational frequency changes upon electronic transition are considered, while neglecting anharmonicities and Duschinsky rotations, which are expected to be small for the cases at hand. Ground-state geometry optimizations and frequency calculations of UO_2Cl_2 were also performed with DFT/PBE using Gaussian 03 with the same basis sets as in the CASPT2 and CCSD(T) calculations above.[34]

The obtained Cartesian force constant matrix was used to construct the *F* matrix of the Wilson−Decius *FG* method[35] for the chosen set of internal coordinates and then combined with the *G* matrix to achieve a normal coordinate analysis. The *F* and *G* matrices were obtained with the help of the program of McIntosh and Peterson.[36,37] The dimensionless geometric displacement parameter upon electronic transition for O−U−O, Δ and the Huang−Rhys factor, *S*,[38] which characterize the overall

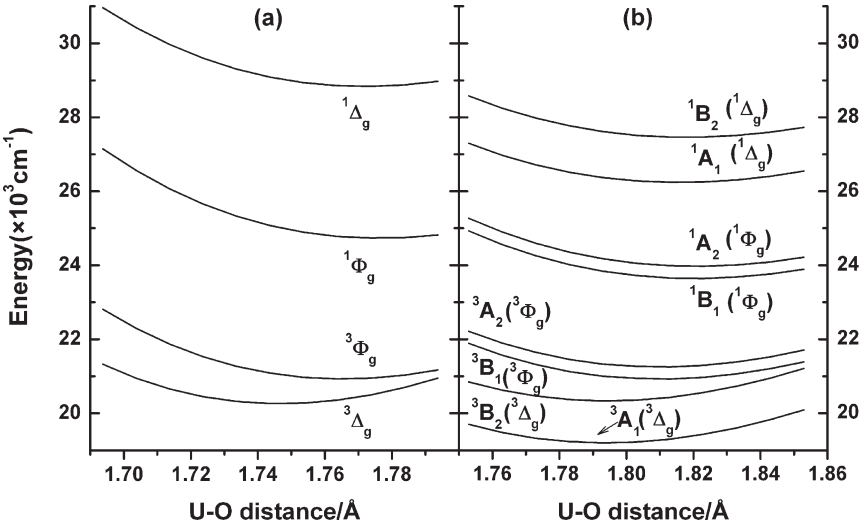

Figure 3. Energy curves of the low-lying excited states of (a) UO_2^{2+} and (b) UO_2Cl_2 for the O−U−O symmetric stretch at the scalar relativistic level from CASPT2 calculations without g_1 correction.

Table 3. Spectroscopic Data from SO-Averaged CASPT2-[g_1] for UO_2^{2+} (g_1 correction in parentheses) and UO_2Cl_2 (g_1' corrected)

molecule	$C_{2v}(D_{\infty h})$	E^a, cm^{-1}	R_e^b, pm	T_e^c, cm^{-1}	ν_s^d, cm^{-1}
UO_2^{2+}	$X^1\Sigma_g^+$		169.35 (0.02)	0 (0)	993 (0)
	$^3\Delta_g$	22 445 (1118)	175.16 (0.32)	21 229 (976)	865 (5)
	$^3\Phi_g$	23 954 (1143)	176.92 (0.36)	21 843 (934)	879 (5)
	$^1\Phi_g$	28 295 (1148)	177.96 (0.46)	25 566 (851)	879 (3)
	$^1\Delta_g$	31 826 (862)	177.59 (0.47)	29 387 (572)	868 (5)
UO_2Cl_2	$X^1A_1(X^1\Sigma_g^+)$		175.27		865
	$a^3A_1(^3\Delta_g)$	20 816	179.82	20 182	757
	$a^3B_2(^3\Delta_g)$	21 962	179.87	21 317	758
	$a^3B_1(^3\Phi_g)$	23 029	181.49	21 855	771
	$a^3A_2(^3\Phi_g)$	23 359	181.51	22 178	771
	$a^1B_1(^1\Phi_g)$	26 075	182.58	24 482	764
	$a^1A_2(^1\Phi_g)$	26 418	182.61	24 809	765
	$a^1A_1(^1\Delta_g)$	28 157	182.16	26 803	739
	$a^1B_2(^1\Delta_g)$	29 441	182.37	28 019	739

[a] Vertical excitation energy E at ground-state geometry. [b] U−O equilibrium distance R_e. [c] Calculated adiabatic excitation energy T_e. [d] O−U−O symmetric stretching frequency ν_s.

shape of the vibrational intensity distribution, were finally obtained from eqs 1−3:

$$FGL = L\Lambda, \qquad L^T F^{-1} L = \Lambda^{-1} \tag{1}$$

$$Q = L^T R, \qquad \Delta Q = L^T \Delta R \tag{2}$$

$$\Delta = \sqrt{(\omega/\hbar)} \cdot \Delta Q, \qquad S = \Delta^2/2 \tag{3}$$

COMPUTATIONAL RESULTS AND DISCUSSION

Optimized Structures of UO_2^{2+} and UO_2Cl_2. As shown in Table 2, the optimized ground-state structures of UO_2^{2+} and UO_2Cl_2 from the CASPT2 and CCSD(T) methods are consistent, both indicating multiple U−O and dative U−Cl bonding. CCSD(T) gives ∼0.4 pm shorter U−O distances but ∼0.2 pm longer U−Cl distances than CASPT2. The expansion of the U−O bonds of uranyl upon equatorial coordination (∼6 pm for two Cl^- ligands) is well understood as equatorial orbital interaction slightly weakening the U−O triple bond in UO_2Cl_2.[39] The bending of the linear OUO unit by ∼14° can be rationalized in terms of 5f-6d-7s hybridization, electrostatic Cl^--O^{2-} repulsion or valence-shell electron-pair repulsion.

The lowest excited states of UO_2Cl_2 are dominated by $\sigma_u \rightarrow \delta_u$ or ϕ_u transitions (Figure 2), similar to those in many other uranyl complexes.[7] The U−O distances of the triplet SO-averaged states are expanded by 4.8 or 6.4 pm, respectively, while the U−Cl distances vary by no more than 1.2 pm. The OUO and ClUCl angles are reduced by 1.3 up to 7.5°.

SO-Averaged Potential Energy Curves of Excited States. *CASPT2 Results.* CASPT2 energy curves of the lowest states of

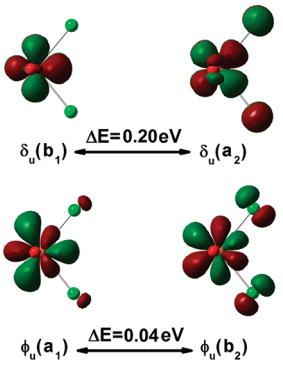

Figure 4. MO isosurfaces (isovalue = 0.03 au) and energies of U-5f δ_u and ϕ_u orbitals of UO_2Cl_2 from DFT/PBE calculations.

Table 4. Spectroscopic Data of UO_2Cl_2 from SO-Averaged CCSD(T) Scan Calculations[a]

state	E, cm^{-1}	R_e, pm	T_e, cm^{-1}	ν_s, cm^{-1}
X^1A_1		174.77		901
a^3A_1	21 389	179.60	20 710 (20 573)	772
		(179.73)		
a^3B_2	22 476	179.58	21 803 (21 764)	773
		(179.45)		
a^3B_1	23 161	180.98	22 003 (21 702)	789
		(181.18)		
a^3A_2	23 514	181.01	22 343 (22 056)	790
		(181.08)		
a^1B_1	26 244	181.92	24 731	785
a^1A_2	26 613	181.95	25 075	788
a^1A_1	29 062	181.71	27 744	755
a^1B_2	30 287	181.81	28 921	756

[a] See footnotes of Table 3. CCSD(T) optimized results in parentheses.

UO_2^{2+} and UO_2Cl_2 arising from the $\sigma_u \rightarrow \delta_u$, ϕ_u excitations at the SO-averaged level are displayed in Figure 3. Respective g_1 and g_1'-corrected numerical spectroscopic data are collected in Table 3. The well-known singlet−triplet splittings of UO_2^{2+}, 9.4 and 4.3 × 10^3 cm^{-1} for the Δ_g and Φ_g, respectively,[17,40] are nearly carried over to UO_2Cl_2 (7.4 and 3.1 × 10^3 cm^{-1}). The chloride ligand-field splittings are 1.2 and 0.3 × 10^3 cm^{-1}. The large $\Delta-\Phi$ difference corresponds to the angular momenta, the shapes, and the orbital energy differences of the U-5fδ_u and U-5fϕ_u type MOs, displayed in Figure 4. Remarkably, there is no combination of Cl-2pπ with U-5fδ_u of B_1 symmetry, also found by Pierloot[17] for the similar case of $UO_2Cl_4^{2-}$, while the Cl-2pσ mixes more strongly with U-5f$\delta_u(A_2)$ than with U-5f$\phi_u(A_1)$.

The O−U−O distances in UO_2Cl_2 are several pm longer than in UO_2^{2+}; correspondingly, the symmetric stretching frequencies ν_s(OUO) are smaller, by 128 cm^{-1} for the ground states and by around 115 cm^{-1} for the excited states. The ν_s values of the excited states are smaller than those of the ground states throughout by more than 100 cm^{-1}, corresponding to the U−O bond length expansion upon electronic excitation. The adiabatic excitation energies of UO_2^{2+} and UO_2Cl_2 differ in the range of −2584 to +335 cm^{-1}.

CCSD(T) Results. Spectral parameters of UO_2Cl_2 from SO-averaged CCSD(T) scans and then fully optimized CCSD(T) are displayed in Table 4. The former reproduces the latter for the excited triplet states quite well, within 2 pm and 300 cm^{-1}. The CCSD(T) scans of the BO energy curves yield reasonable approximations to the CCSD(T) optimized results. We expect similarly reliable results from the CASPT2 scans.

The U−O bond lengths of the ground and excited states from CCSD(T) in Table 4 are around 0.5 pm shorter than the CASPT2-[g_1'] results in Table 3. The excitation energies in Table 4 are larger than the CASPT2 values by 150 to 950 cm^{-1}, and the ν_s values are larger: 38 cm^{-1} for the ground state, 20 cm^{-1} for the excited Φ_g type states, and 16 cm^{-1} for the excited Δ_g type states. These results illustrate the accuracy of the theoretical results.

Spin−Orbit Coupled States. *RASSCF/CASPT2/SO Results.* SO-coupled BO-energy curves of the low-lying excited states of UO_2^{2+} and UO_2Cl_2 along the O−U−O symmetric stretch are presented in Figure 5. These curves are derived from the spin triplets and are calculated with CASPT2. The g_1 and g_1'-corrected numerical data with Ω-values are collected in Table 5. The SO-splittings of the states of $^3\Delta_g$ type are rather regular and of the order of 2 × 10^3 cm^{-1}. The SO splittings of the $^3\Phi_g$ type states are larger due to the larger orbital angular momentum component (nearly 6 × 10^3 cm^{-1}) and less regular due to more pronounced interaction of e−e and SO configuration mixing. As a result, the lowest excited state is dominated by $^3\Phi_g$ character.[7,17,18,40a]

Literature results on the lowest excited, luminescent state of UO_2^{2+} are also displayed in Table 5. Our results agree better with those of Pierloot and van Besien[17] than with those of Zhang and Pitzer[15] or Réal at al.,[40] concerning the $^3\Phi_g$ character, the U−O bond length expansion and the excitation energy. From the experimental adiabatic excitation energy of ∼20 323 cm^{-1} and the deduced U−O bond length expansion of the luminescent state of ∼5.8 pm and the respective errors of the CASPT2 calculation of UO_2Cl_2, the most probable values for UO_2^{2+} are deduced to be 20 434 cm^{-1} and 7.5 pm, consistent with the best excitation energy given by Vallet[40a] and the best U−O bond length expansion by Pierloot.[17] As usual,[40b] the calculated luminescence parameters are influenced by the different basis sets and the treatment of electron correlation and relativistic effects.

While there is no excited-state calculations on UO_2Cl_2, theoretical results on related $UO_2Cl_2(ac)_3$ (ac = acetone) are known.[19] Inasmuch as stronger ligand interactions in the equatorial plane destabilize $^3\Phi_g$ type states in comparison to $^3\Delta_g$ ones,[7,17,41] the lowest excited state of $UO_2Cl_2(ac)_3$ was found to be ($^3\Delta_g$)aA_2 with a vertical energy around 20.3 × 10^3 cm^{-1}, i.e., higher than for UO_2Cl_2.

RASSCF/CCSD(T)/SO Results. RASSCF/CCSD(T)/SO results for UO_2Cl_2 are displayed in Table 6 and are similar to the RASSCF/CASPT2-[g_1']/SO ones. Comparing with the CASPT2 results, the CCSD(T) approach yields up to 0.6 pm smaller U−O distances, 160 to 525 cm^{-1} higher exciation energies, and 5 to 30 cm^{-1} larger vibration frequencies. These differences are also found at the SO-averaged level (Tables 3 and 4).

Influence of the Ar Matrix. *Structures, Binding Energies, and Excited States of $Ar_nUO_2Cl_2$.* As weak Lewis bases, argon atoms can bind to actinide metal atoms at lower temperatures. For instance, the coordination of Ar atoms to CUO and UO_2 has been shown to cause so-called ground-state reversal in comparison to gas-phase or neon matrix results.[42−46]

Since Ar is a much weaker Lewis base than carbonyl or carboxyl ligands, oxophilic uranyl is expected to be only weakly

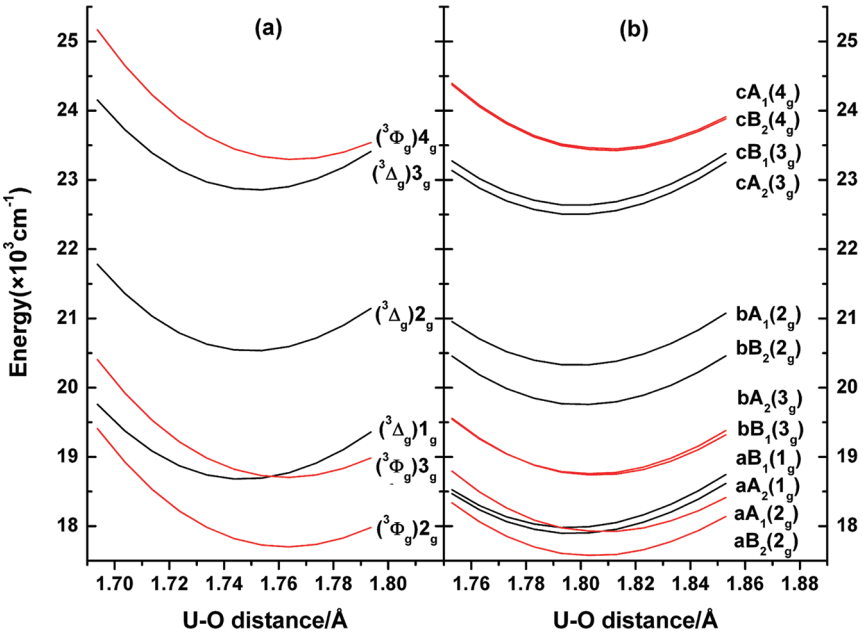

Figure 5. Energy curves of excited states of (a) UO_2^{2+} and (b) UO_2Cl_2 along the O−U−O symmetric stretch coordinate from CASPT2 with SO coupling, without g_1-correction (red curves: $^3\Phi$ type; black curves: $^3\Delta$ type).

Table 5. Spectroscopic Data from SO-Coupled CASPT2-[g_1] for UO_2^{2+} (g_1 correction in parentheses) and UO_2Cl_2 (g_1' corrected)[a]

molecule	state (Ω)	main[b]	E, cm^{-1}	R_e, pm	ΔR_e, pm[c]	T_e, cm^{-1}	ν_s, cm^{-1}
UO_2^{2+}	$X\Sigma_g^+$ (0_g^+)			169.35 (0.02)		0 (0)	993 (0)
	$a\Delta_g$ (2_g)	$^3\Phi_g$	20 543 (1134)	176.71 (0.37)	+7.36	18 620 (937)	862 (3)
	Π_g (1_g)	$^3\Delta_g$	20 877 (1118)	175.19 (0.32)	+5.84	19 648 (975)	866 (6)
	$a\Phi_g$ (3_g)	$^3\Phi_g$	21 541 (1135)	176.71 (0.37)	+7.36	19 618 (932)	862 (4)
	$b\Delta_g$ (2_g)	$^3\Delta_g$	22 892 (1110)	175.49 (0.32)	+6.14	21 471 (950)	886 (6)
	$b\Phi_g$ (3_g)	$^3\Delta_g$	25 282 (1127)	175.65 (0.33)	+6.30	23 809 (966)	880 (6)
	Γ_g (4_g)	$^3\Phi_g$	26 312 (1144)	176.90 (0.35)	+7.55	24 211 (935)	878 (4)
Pierloot[17]	$a\Delta_g$ (2_g)	$^3\Phi_g$	19 195		7.4	17 227	815
Vallet[40a]	$a\Delta_g$ (2_g)	$^3\Phi_g$	22 789		6.4	21 338	963
Pitzer[15]	Π_g (1_g)	$^3\Delta_g$			6.5	20 719	867
Vallet[40b]	Π_g (1_g)	$^3\Delta_g$	18 610		4.1	17 557	
UO_2Cl_2	XA_1(0_g)			175.27			865
	aB_2 (2_g)	$^3\Phi_g$	19 471	180.97	+5.70	18 509	752
	aA_1 (2_g)	$^3\Phi_g$	19 928	181.30	+6.03	18 850	760
	aA_2 (1_g)	$^3\Delta_g$	19 587	180.25	+4.98	18 874	741
	aB_1 (1_g)	$^3\Delta_g$	19 644	180.11	+4.84	18 961	743
	bB_1 (3_g)	$^3\Phi_g$	20 693	181.04	+5.77	19 666	772
	bA_2 (3_g)	$^3\Phi_g$	20 681	180.90	+5.63	19 686	776
	bB_2 (2_g)	$^3\Delta_g$	21 567	180.55	+5.28	20 706	775
	bA_1 (2_g)	$^3\Delta_g$	22 065	180.33	+5.06	21 278	766
	cA_2 (3_g)	$^3\Delta_g$	24 262	180.34	+5.07	23 470	768
	cB_1 (3_g)	$^3\Delta_g$	24 401	180.37	+5.10	23 602	769
	cB_2 (4_g)	$^3\Phi_g$	25 519	181.46	+6.19	24 351	769
	cA_1 (4_g)	$^3\Phi_g$	25 538	181.45	+6.18	24 374	770
$UO_2Cl_2ac_3$[d]	aA_2 (1_g)	$^3\Delta_g$	20 338				

[a] See footnotes of Table 3. [b] Main component of wave function . [c] U−O bond length expansion upon electronic excitation. [d] See ref 19, ac = acetone.

perturbed by Ar. We simulate the argon matrix effect by $Ar_nUO_2Cl_2$ complexes, neglecting additional soft lattice effects.

Structures of $Ar_nUO_2Cl_2$ molecules (n = 0−4) exhibiting C_{2v} symmetry were optimized by using DFT/PBE and CCSD(T)

with basis set superposition error (BSSE) correction. From the binding energies shown in Figure 6, the most stable species are $Ar_2UO_2Cl_2$ and $Ar_3UO_2Cl_2$. These species were chosen to simulate the Ar matrix effects on the UO_2Cl_2 spectra and their structural parameters from CCSD(T) and CASPT2 calculations are displayed in Table 7.

The binding energy per Ar atom is 10 and 5.5 kJ/mol in $Ar_2UO_2Cl_2$ and $Ar_3UO_2Cl_2$, respectively. The U−Ar distances of 3.1−3.4 Å are consistent with van der Waals binding. Equatorial coordination of Ar atoms expands the U−O distances, albeit only by 0.1 pm per Ar. The O−U−O bending due to the Cl ligands is slightly reduced by Ar atoms in the trans position. The Cl−U−Cl angle is reduced by about 8° in $Ar_3UO_2Cl_2$ but unexpectedly widened by some 5° in $Ar_2UO_2Cl_2$.

Since RASSCF/CASPT2-[g_1']/SO and RASSCF/CCSD(T)/SO give consistent results, only the latter are displayed in Table 8 for the cases of zero-, two-, and three-coordinated Ar atoms. The electronic excitation patterns of the three species are quite similar. The argon environment increases the first adiabatic excitation energy by a few 100 cm^{-1}. The higher excitation energies also vary a little. The OUO symmetric stretching frequencies vary in the order of ±10 cm^{-1}, indicating that Ar-coordination insignificantly affects these uranyl complexes.

Luminescence of $Ar_nUO_2Cl_2$. The luminescent state properties of $Ar_nUO_2Cl_2$ (n = 0, 2, 3) are collected in Table 9. As mentioned before, Ar coordination does not change the dominance of $^3\Phi_g$ character, in contrast to complexes perturbed by carbonyl or carboxyl ligands.[7,19] Also the U−O bond length changes upon electronic transition, and the vibrational frequencies, i.e. the overall spectral shapes, are insignificantly modified by the Ar ligands. Increases of vertical and adiabatic transition energies of around 450 cm^{-1} for dicoordination and of around 100 cm^{-1} for tricoordination are consistently predicted by RASSCF/CASPT2-[g_1']/SO and RASSCF/CCSD(T)/SO approaches within ±100 cm^{-1}. The electronic transition dipole moments μ of the fluorescence are reduced by factors of 0.4−0.7 due to the Ar coordination.

Heaven et al.[8] had experimentally found a biexponential decay in the argon matrix with lifetimes of 50 and 260 μs. They had related it to two matrix sites differing in the nonradiative decay times. Assuming the same optical transition probability for both sites, the more rapidly decaying site would have been populated more by a factor of about 4.2. Since the Ar-coordinated complexes have optical transition probabilities differing by factors of κ = 1.6−2.1 in the two applied quantum chemical approaches, the deduced population ratio of 4.2:1 should be raised or lowered by that κ factor around 2.

The optical oscillator strengths f are of the order of 10^{-6}, which is common for forbidden transitions in transition-metal complexes. The respective lifetimes are a fraction of a second (s), while the measured ones are a fraction of a ms. Therefore the decay mechanism is dominated indeed by nonradiative transitions. The optical lifetime was estimated by eq 4:[1]

$$\tau_{optical} = 3\pi\varepsilon_0\hbar{c_n}^3/\omega^3\mu^2 \quad (4)$$

where ε_0 is the electric permittivity in vacuum, $\hbar$ the reduced Planck constant, c_n the velocity of light in solid argon, ω the angular frequency, and μ the electric transition dipole moment.

Table 6. Spectroscopic data of UO_2Cl_2 from RASSCF/CCSD(T)/SO[a]

state (Ω)	main	E, cm^{-1}	R_e, pm	ΔR_e, pm	T_e, cm^{-1}	ν_s, cm^{-1}
XA_1 (0_g)			174.77			901
aB_2 (2_g)	$^3\Phi_g$	19 804	180.66	+5.89	18 797	775
aA_1 (2_g)	$^3\Phi_g$	20 157	180.87	+6.10	19 060	782
aA_2 (1_g)	$^3\Delta_g$	20 106	180.20	+5.43	19 297	752
aB_1 (1_g)	$^3\Delta_g$	20 183	180.05	+5.28	19 422	748
bB_1 (3_g)	$^3\Phi_g$	20 991	180.47	+5.70	19 986	802
bA_2 (3_g)	$^3\Phi_g$	20 983	180.33	+5.56	20 030	799
bB_2 (2_g)	$^3\Delta_g$	21 977	180.12	+5.35	21 121	786
bA_1 (2_g)	$^3\Delta_g$	22 537	179.95	+5.18	21 746	778
cB_1 (3_g)	$^3\Delta_g$	24 801	179.97	+5.20	23 995	783
cA_2 (3_g)	$^3\Delta_g$	24 659	179.96	+5.19	23 862	781
cB_2 (4_g)	$^3\Phi_g$	25 665	180.97	+6.20	24 511	789
cA_1 (4_g)	$^3\Phi_g$	25 686	180.95	+6.18	24 536	789

[a] See footnotes of Tables 3 and 5.

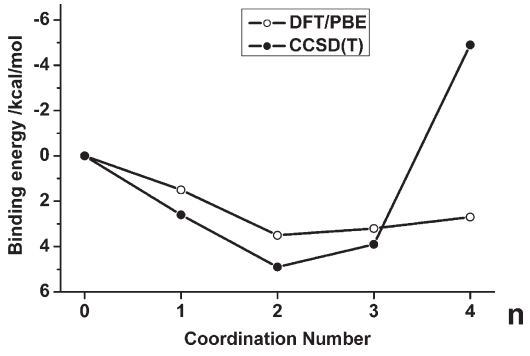

Figure 6. Binding energies of $Ar_nUO_2Cl_2$ ground-state species formed from UO_2Cl_2 + n Ar, from CCSD(T) (with BSSE correction) and from DFT/PBE calculations.

Table 7. Geometric Ground-State Parameters of $Ar_nUO_2Cl_2$ Complexes

complex	R_{U-O}, pm	R_{U-Cl}, pm	∠OUO, °	∠ClUCl, °	R_{U-Ar}, pm	$R_{U-Ar'}$, pm
			CASPT2			
UO_2Cl_2	175.29	249.12	165.83	106.76		
$Ar_2UO_2Cl_2$	175.47	250.46	168.24	112.19	308.37	
$Ar_3UO_2Cl_2$	175.63	249.53	167.14	98.40	339.92	323.67
			CCSD(T)			
UO_2Cl_2	174.77	250.92	165.76	107.73		
$Ar_2UO_2Cl_2$	174.91	252.15	168.17	112.21	312.29	
$Ar_3UO_2Cl_2$	175.03	251.35	166.93	99.34	346.92	327.68

Table 8. Spectroscopic Data of $Ar_nUO_2Cl_2$ (n = 0, 2, 3) from RASSCF/CCSD(T)/SO Calculations[a]

		UO_2Cl_2		$Ar_2UO_2Cl_2$		$Ar_3UO_2Cl_2$	
state (Ω)	main	T_e, cm^{-1}	ν_s, cm^{-1}	T_e, cm^{-1}	ν_s, cm^{-1}	T_e, cm^{-1}	ν_s, cm^{-1}
aB_2 (2_g)	$^3\Phi_g$	18 797	775	19 364	770	18 942	769
aA_1 (2_g)	$^3\Phi_g$	+263	782	+353	776	+332	775
aA_2 (1_g)	$^3\Delta_g$	+500	752	+357	752	+432	749
aB_1 (1_g)	$^3\Delta_g$	+625	748	+453	756	+498	747
bB_1 (3_g)	$^3\Phi_g$	+1189	802	+1220	786	+1192	792
bA_2 (3_g)	$^3\Phi_g$	+1233	799	+1184	790	+1266	790
bB_2 (2_g)	$^3\Delta_g$	+2324	786	+2308	785	+2284	782
bA_1 (2_g)	$^3\Delta_g$	+2949	778	+2670	776	+2837	771
cB_1 (3_g)	$^3\Delta_g$	+5198	783	+5106	782	+5106	778
cA_2 (3_g)	$^3\Delta_g$	+5065	781	+4910	779	+5066	777
cB_2 (4_g)	$^3\Phi_g$	+5714	789	+5887	787	+5818	784
cA_1 (4_g)	$^3\Phi_g$	+5739	789	+5917	787	+5823	785

[a] See footnotes of Tables 3 and 5.

Table 9. Data of the Luminescent States of $Ar_nUO_2Cl_2$ (n = 0, 2, 3) from RASSCF/CASPT2-[g_1']/SO and RASSCF/CCSD(T)/SO Calculations[a]

molecule	state (Ω)	main	E, cm^{-1}	ΔR_e, pm	T_e, cm^{-1}	$\mu \times 10^3$, au	ν_s, cm^{-1}
			CASPT2-[g_1']				
UO_2Cl_2	aB_2 (2_g)	$^3\Phi_g$	19 471	+5.70	18 509	6.73	752
$Ar_2UO_2Cl_2$	aB_2 (2_g)	$^3\Phi_g$	19 844	+5.77	18 869	2.48	747
$Ar_3UO_2Cl_2$	aB_2 (2_g)	$^3\Phi_g$	19 539	+5.69	18 591	3.58	744
			CCSD(T)				
UO_2Cl_2	aB_2 (2_g)	$^3\Phi_g$	19 804	+5.89	18 797	9.99	775
$Ar_2UO_2Cl_2$	aB_2 (2_g)	$^3\Phi_g$	20 378	+5.95	19 363	5.94	770
$Ar_3UO_2Cl_2$	aB_2 (2_g)	$^3\Phi_g$	19 947	+5.93	18 942	7.44	769

[a] See footnotes of Tables 3 and 5, and μ = electronic transition dipole moment between ground and lowest excited states in au at the geometry of the latter.

Table 10. Electronic Excitation Spectra of UO_2Cl_2 from Calculations (RASSCF/CASPT2-[g_1']/SO, RASSCF/CCSD(T)/SO) and Experiments[a]

		T_e, cm^{-1}	ν_s, cm^{-1}	$\mu \times 10$, au	T_e, cm^{-1}	ν_s, cm^{-1}	$\mu \times 10^3$, au	T_e, cm^{-1}	ν_s, cm^{-1}	int[b]
		CASPT2-[g_1']			CCSD(T)			exptl.[c]		
state (Ω)	main									
XA_1 (0_g)			865			901			840	
aB_2 (2_g)	$^3\Phi_g$	18 509	752	2.28	18 797	775	5.90	20 359	717	w
aA_1 (2_g)	$^3\Phi_g$	+341	760	7.04	+263	782	7.75	+516	706	w
aA_2 (1_g)	$^3\Delta_g$	+365	741	0	+500	752	0			
aB_1 (1_g)	$^3\Delta_g$	+452	743	0.31	+625	748	0.43			
bB_1 (3_g)	$^3\Phi_g$	+1157	772	0.79	+1189	802	0.90	+966	713	w
bA_2 (3_g)	$^3\Phi_g$	+1177	776	0	+1233	799	0			
bB_2 (2_g)	$^3\Delta_g$	+2197	775	51.42	+2324	786	49.58	+2310	709	s
bA_1 (2_g)	$^3\Delta_g$	+2769	766	24.04	+2949	778	22.98	+2522	713	s

[a] See footnotes of Tables 3, 5, and 9 (with μ at the ground-state geometry). [b] Int: observed intensity, w = weak, and s = strong. [c] Absorption by UO_2Cl_2 in an Ar matrix.

Assignment and Simulation of Experimental Spectra. *Assignment of the Experimental Excitation Spectra.* Heaven et al.[8] had identified 5 progressions in the absorption spectrum of UO_2Cl_2/argon matrix in the range of 20−24 × 10^3 cm^{-1}. In Table 10, we contrast their data with our calculated results for the eight lowest excited states of UO_2Cl_2 in that energy range. Transitions to the two excited states of A_2 symmetry are electronic-dipole forbidden, and the one to the lower state of B_1 symmetry has a distinctively

low calculated intensity; these transitions were too weak to be detected in the mentioned experiment.

Table 11. Vibrational Normal-Mode Coordinates of OUO Symmetric Stretch (s) and Bend (b) in UO_2Cl_2 from DFT/PBE Frequency Calculations

	normal coordinate, unit: $(g/mol)^{1/2}$	
internal coordinates, unit: Å or Å × rad	s (OUO)	b (OUO)
$R(U_1-O_2)$	2.82	0.04
$R(U_1-O_3)$	2.82	0.04
$R(U_1-Cl_4)$	0.17	0.83
$R(U_1-Cl_5)$	0.17	0.83
$\angle(O_2-U_1-O_3)$	0.12	−3.41
$\angle(O_2-U_1-Cl_4)$	−0.04	1.01
$\angle(O_2-U_1-Cl_5)$	−0.04	1.01
$\angle(O_3-U_1-Cl_4)$	−0.04	1.01
$\angle(O_3-U_1-Cl_5)$	−0.04	1.01
$\angle(Cl_4-U_1-Cl_5)$	0.02	0.88

Table 12. Parameters for Luminescence Spectra Simulation of UO_2Cl_2

parameter[a]	CASPT2-[g_1']	CCSD(T)	exptl.
ΔR(U−O), pm	+5.70	+5.89	
$\Delta(\angle$OUO), °	−3.33	−5.96	
$\Delta(\angle$ClUCl), °	−2.96	−5.57	
$\Delta(\angle$OUCl), °	+1.17	+2.13	
ν_s^g (OUO), cm^{-1}	865	901	839
ν_s^e (OUO), cm^{-1}	752	775	717
ν_b^g (OUO), cm^{-1}	185[b]	214	242
ΔQ_s, Å·$(g/mol)^{1/2}$	0.31	0.31	
ΔQ_b, Å·$(g/mol)^{1/2}$	0.24	0.42	
T_e, cm^{-1}	18 509	18 797	20 323
band width, cm^{-1}			63

[a] Changes of geometrical parameters between the ground and luminescent state; ν_s^g and ν_b^g are the symmetric stretching and bending frequencies of the ground state; ν_s^e is the stretching frequency of the luminescent state; and ΔQ_s and ΔQ_b are the corresponding normal coordinate displacements. See footnotes of Table 3 for T_e. [b] From DFT/PBE calculations.

Among the remaining 5 calculated transitions, the lower 3 transitions of $(^3\Phi_g)B_2(2_g)$, $(^3\Phi_g)A_1(2_g)$, and $(^3\Phi_g)B_1(3_g)$ type have medium oscillator strengths of $0.04-3.5 \times 10^{-6}$, while those of $(^3\Delta_g)B_2(2_g)$ and $(^3\Delta_g)A_1(2_g)$ type at higher energy have higher oscillator strengths of $35-167 \times 10^{-6}$. Indeed, experimentally three week transitions at lower energies and two strong transitions at higher energies were detected. The calculated energy pattern of these 5 excitations, distributed over nearly 3000 cm^{-1}, is in agreement with experiment within ±300 cm^{-1}, although the calculated absolute excitation energies are on the average ∼1400 cm^{-1} too low. This value of less than 0.2 eV is within the accuracy of present-day computational approaches. The calculated excited-state harmonic vibrational frequencies of the symmetric O−U−O stretch are consistently 8% high.

The reasonable agreement corroborates the reliability of the above given assignments of the electronic excitations. With these theoretical results we can improve the previous tentative assignment[8] with respect to the symmetry species (B_1 or B_2) and the dominant $D_{\infty h}$ term values ($^3\Delta_g$ or $^3\Phi_g$) and angular momenta ($\Omega = 1, 2,$ or 3). Namely, the original assignments were based on the calculated vertical excitation energies of $UO_2Cl_2(ac)_3$,[19] while we have now found that UO_2Cl_2 in an argon matrix is much less perturbed than in acetone solution.

Simulation of the Experimental Luminescence Spectra. Because the Ar matrix effects on the vibrational frequencies and bond lengths are so weak, we may simulate the shapes of the luminescence spectra with the help of the calculated data for free UO_2Cl_2. Because at present the calculated absolute excitation energies are still not spectroscopically accurate and the prediction of homogeneous and heterogeneous line broadening effects is still too complicated, these two parameters will be adjusted to the experiments.

The two spectroscopically most important, totally symmetric vibrational modes are specified in Table 11. The character is O−U−O stretching and, respectively, a mix of O−U−O and O−U−Cl bending. The other symmetric vibrations, including Cl−U−Cl and Ar−U−Ar stretching and bending modes, are found not to contribute markedly to the shape of the spetra due to the small displacements and/or frequencies.

All numerical parameters for the spectral simulations are assembled in Table 12, and the correspondingly simulated spectra are shown in Figure 7. The experimental emission spectrum[8] is dominated by a progression of the symmetric O−U−O stretching vibration of 839 cm^{-1} of the electronic ground state. Each band has a weak foot lower by 242 cm^{-1},

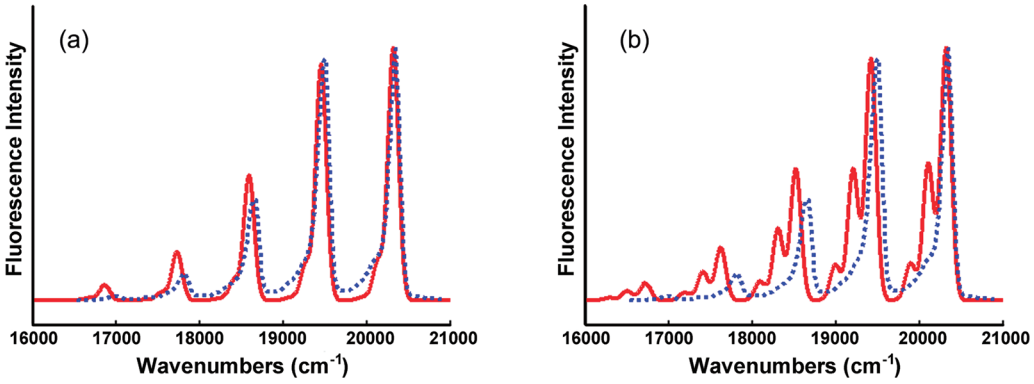

Figure 7. Simulated (red) and experimental (blue) luminescence spectra of UO_2Cl_2: (a): RASSCF/CASPT2-[g_1']/SO and (b): RASSCF/CCSD(T)/SO.

corresponding to O−U−O bending. Our calulations corroborate the experimental assignments, with the addition that the bending vibration is a blend of U−O and U−Cl bendings. The CCSD(T) approach seems to exaggerate the intensity of the bending mode, due to the large geometric changes Δ (Table 12), and also yielded the largest ground-state vibrational frequency, which results in the pronounced red shift of the progression (Figure 7).

CONCLUSIONS

We have investigated UO_2Cl_2 in an argon matrix using ab initio RASSCF/CASPT2/SO and RASSCF/CCSD(T)/SO approaches. The electronically excited states and spectra in the near UV−vis region <27 000 cm^{-1} are calculated and interpreted. UO_2Cl_2 interacting with an argon matrix is approximated by $Ar_nUO_2Cl_2$ complexes, where Ar acts as a very weak Lewis base. Two structures (n = 2 and 3, Figure 1) are particularly stable, corresponding to the two different matrix sites experimentally deduced and now specified. The luminescence spectra are approximately reproduced theoretically, giving confidence in the theoretical assignments. Accordingly, the fluorescent lowest excited state of UO_2Cl_2 with weakly interacting Ar atoms is of $(U\text{-}5f\phi_u\ ^3\Phi_g)B_2(2_g)$ character, in contrast to $(U\text{-}5f\delta_u\ ^3\Delta_g)B_1(1_g)$ of UO_2Cl_2 with equatorial oxygen ligands, such as carbonyl or carboxyl groups. The spectroscopic U−O bond length expansion of UO_2Cl_2 upon electronic excitation from the bonding σ_u-HOMO → the nonbonding U-5fϕ_u-LUMO of $\Delta R_{UO} \approx$ 5.8 pm is reproduced by the CASPT2 and CCSD(T) approaches. The bending vibrational frequencies and bond angle changes are theoretically exaggerated by CCSD(T). The absolute intensities, depending both on SO-coupling and geometric asymmetry and on vibronic coupling and radiationless processes, are not calculated. The synergic combination of experimental and theoretical works has helped to eliminate deficiencies of both approaches.

AUTHOR INFORMATION

Corresponding Author

*E-mail: junli@mail.tsinghua.edu.cn.

Present Addresses

‡Mailing Address of W.H.E.S: Theoretical Chemistry, University of Siegen, 57068 Siegen, Germany. E-mail: schwarz@chemie.uni-siegen.de.

ACKNOWLEDGMENT

The authors thank H. Stoll and M. Dolg for helpful comments. This work was financially supported by the NKBRSF (2011CB932400) and NSFC (20933003, 11079006, 91026003) of China. The calculations were performed by using computers at the Supercomputing Center of the Computer Network Information Center, Chinese Academy of Sciences, and the Shanghai Supercomputing Center. A portion of calculations was performed using EMSL, a national scientific user facility sponsored by the U.S. Department of Energy's Office of Biological and Environmental Research and located at the Pacific Northwest National Laboratory, Richland, WA.

REFERENCES

(1) Rabinowitch, E.; Belford, R. L. *Spectroscopy and Photoechemistry of Uranyl Compounds*; Oxford University Press, Oxford, U.K., 1964.

(2) Pepper, M.; Bursten, B. E. *Chem. Rev.* **1991**, *91*, 719–741.

(3) Ghosh, R.; Mondal, J. A.; Ghosh, H. N.; Palit, D. K. *J. Phys. Chem. A* **2010**, *114*, 5263–5270.

(4) Szabó, Z.; Toraishi, T.; Vallet, V.; Grenthe, I. *Coord. Chem. Rev.* **2006**, *250*, 784–815.

(5) (a) Taylor, D. M. *J. Alloys Compd.* **1998**, *271−273*, 6–10. (b) Guilmette, R. A. *J. Alloys Compd.* **1998**, *271−273*, 66–71. (c) Stradling, G. N. *J. Alloys Compd.* **1998**, *271−273*, 72–77.(d) Wolf, S. F. In *The Chemistry of the Actinide and Transactinide Elements*, 3rd ed.; Morss, L. R., Edelstein, N. M., Fuger, J., Katz, J. J., Eds.; Springer: Dordrecht, The Netherlands, 2006; Vol. 5, Chapter 30. (e) Durbin, P. W. In *The Chemistry of the Actinide and Transactinide Elements*, 3rd ed.; Morss, L. R., Edelstein, N. M., Fuger, J., Katz, J. J., Eds.; Springer: Dordrecht, The Netherlands, 2006; Vol 5, Chapter 31.

(6) (a) Szigethy, G.; Xu, J.; Gorden, A. E. V.; Teat, S. J.; Shuh, D. K.; Raymond, K. N. *Eur. J. Inorg. Chem.* **2008**, 2143–2147. (b) Gorden, A. E. V.; Xu, J.; Szigethy, G.; Oliver, A.; Shuh, D. K.; Raymond, K. N. *J. Am. Chem. Soc.* **2007**, *129*, 6674–6675. (c) Gramer, C. J.; Raymond, K. N. *Inorg. Chem.* **2004**, *43*, 6397–6402. (d) Veeck, A. C.; White, D. J.; Whisenhunt, D. W., Jr.; Xu, J.; Gorden, A. E. V.; Romanovski, V.; Hoffman, D. C.; Raymond, K. N. *Solvent Extr. Ion Exch.* **2004**, *22*, 1037–1068. (e) Xu, J.; Gorden, A. E. V.; Raymond, K. N. *Eur. J. Org. Chem.* **2004**, 3244–3253. (f) Guilmette, R. A.; Hakimi, R.; Durbin, P. W.; Xu, J.; Raymond, K. N. *Radiat. Prot. Dosim.* **2003**, *105*, 527–534. (g) Gorden, A. E. V.; Xu, J.; Raymond, K. N.; Durbin, P. W. *Chem. Rev.* **2003**, *103*, 4207–4282. (h) Xu, J.; Durbin, P. W.; Kullgren, B.; Ebbe, S. N.; Uhlir, L. C.; Raymond, K. N. *J. Med. Chem.* **2002**, *45*, 3963–3971.

(7) Su, J.; Zhang, K.; Schwarz, W. H. E.; Li, J. *Inorg. Chem.* **2011**, *50*, 2082–2093.

(8) Jin, J.; Gondalia, R.; Heaven, M. C. *J. Phys. Chem. A* **2009**, *113*, 12724–12728.

(9) Denning, R. G. *J. Phys. Chem. A* **2007**, *111*, 4125–4143.

(10) (a) Denning, R. G.; Snellgrove, T. R.; Woodwark, D. R. *Mol. Phys.* **1976**, *32*, 419–442. (b) Barker, T. J.; Denning, R. G.; Thorne, J. R. G. *Inorg. Chem.* **1987**, *26*, 1721–1732.

(11) Flint, C. D.; Tanner, P. A. *J. Chem. Soc., Faraday Trans. 2* **1978**, *74*, 2210–2217.

(12) Görller-Walrand, C.; de Houwer, S.; Fluyt, L.; Binnemans, K. *Phys. Chem. Chem. Phys.* **2004**, *6*, 3292–3298.

(13) Li, J.; Bursten, B. E. In *Computational Organometallic Chemistry*; Cundari, T. R., Ed.; Marcel Dekker: New York, 2001; pp 345−379.

(14) Li, J.; Burtsen, B. E. *J. Am. Chem. Soc.* **1998**, *120*, 11456–11466.

(15) Zhang, Z.; Pitzer, R. M. *J. Phys. Chem. A* **1999**, *103*, 6880–6886.

(16) Matsika, S.; Pitzer, R. M. *J. Phys. Chem. A.* **2001**, *105*, 637–645.

(17) Pierloot, K.; van Besien, E. *J. Chem. Phys.* **2005**, *123*, 204309.

(18) Pierloot, K.; van Besien, E.; van Lenthe, E.; Baerends, E. J. *J. Chem. Phys.* **2007**, *126*, 194311.

(19) van Besien, E.; Pierloot, K.; Görller-Walrand, C. *Phys. Chem. Chem. Phys.* **2006**, *8*, 4311–4319.

(20) Werner, H. J. *MOLPRO*, version 2008.1; University College Cardiff Consultants Limited: Cardiff, U.K.; http://www.molpro.net

(21) (a) *Amsterdam Density Functional (ADF)* 2009.01; Scientific Computing and Modeling: Amsterdam, The Netherlands; http://www.scm.com. (b) Fonseca Guerra, C.; Snijders, J. G.; te Velde, G.; Baerends, E. J. *Theor. Chem. Acc.* **1998**, *99*, 391–403. (c) te Velde, G.; Bickelhaupt, F. M.; van Gisbergen, S. J. A.; Fonseca Guerra, C.; Baerends, E. J.; Snijders, J. G.; Ziegler, T. *J. Comput. Chem.* **2001**, *22*, 931–967.

(22) (a) Weigand, A.; Cao, X.-Y.; Vallet, V.; Flament, J.-P.; Dolg, M. *J. Phys. Chem. A* **2009**, *113*, 11509–11516. (b) Dolg, M.; Cao, X.-Y. *J. Phys. Chem. A* **2009**, *113*, 12573–12581.

(23) (a) *Pseudopotentials, ECPs*; University of Stuttgart: Stuttgart, Germany. http://www.theochem.uni-stuttgart.de/pseudopotentials. (b) Nicklass, A.; Dolg, M.; Stoll, H.; Preuß, H. *J. Chem. Phys.* **1995**, *102*, 8942–8952.

(24) Krishnan, R.; Binkley, J. S.; Seeger, R.; Pople, J. A. *J. Chem. Phys.* **1980**, *72*, 650–654.

(25) (a) van Lenthe, E.; Ehlers, A. E.; Baerends, E. J. *J. Chem. Phys.* **1999**, *110*, 8943–8953. (b) van Lenthe, E.; Baerends, E. J.; Snijders, J. G.

J. Chem. Phys. **1994**, *101*, 9783–9792. (c) van Lenthe, E.; Baerends, E. J; Snijders, J. G. *J. Chem. Phys.* **1993**, *99*, 4597–4610. (d) van Lenthe, E.; Snijders, J. G.; Baerends, E. J. *J. Chem. Phys.* **1996**, *105*, 6505–6516. (e) van Lenthe, E.; van Leeuwen, R.; Baerends, E. J.; Snijders, J. G. *Int. J. Quantum Chem.* **1996**, *57*, 281–293.

(26) Wei, F.; Wu, G. S.; Schwarz, W. H. E.; Li, J. *Theor. Chem. Acc.* **2011**, *129*, 467–481.

(27) Malmqvist, P. Å.; Roos, B. O.; Schimmelpfennig, B. *Chem. Phys. Lett.* **2002**, *357*, 230–240.

(28) Roos, B. O.; Malmqvist, P. Å. *Phys. Chem. Chem. Phys.* **2004**, *6*, 2919–2927.

(29) Wei, F.; Wu, G. S.; Schwarz, W. H. E.; Li, J. *J. Chem. Theory Comput.* **2011**, DOI: 10.1021/ct2000233.

(30) Wang, X. B.; Wang, Y.-L.; Yang, J.; Xing, X.-P.; Li, J.; Wang, L. S. *J. Am. Chem. Soc.* **2009**, *131*, 16368–16370.

(31) Wang, Y.-L.; Zhai, H. J.; Xu, L.; Li, J.; Wang, L. S. *J. Phys. Chem. A* **2010**, *114*, 1247–1254.

(32) Wang, Y.-L.; Wang, X. B.; Xing, X. -P.; Wei, F.; Li, J.; Wang, L. S. *J. Phys. Chem. A* **2010**, *114*, 11244–11251.

(33) Fonger, W. H.; Struck, C. W. *J. Chem. Phys.* **1974**, *60*, 1994–2002.

(34) Frisch, M. J.; Trucks, G. W.; Schlegel, H. B.; Scuseria, G. E.; Robb, M. A.; Cheeseman, J. R.; Montgomery, J. A., Jr.; Vreven, T.; Kudin, K. N.; Burant, J. C.; Millam, J. M.; Iyengar, S. S.; Tomasi, J.; Barone, V.; Mennucci, B.; Cossi, M.; Scalmani, G.; Rega, N.; Petersson, G. A.; Nakatsuji, H.; Hada, M.; Ehara, M.; Toyota, K.; Fukuda, R.; Hasegawa, J.; Ishida, M.; Nakajima, T.; Honda, Y.; Kitao, O.; Nakai, H.; Klene, M.; Li, X.; Knox, J. E.; Hratchian, H. P.; Cross, J. B.; Bakken, V.; Adamo, C.; Jaramillo, J.; Gomperts, R.; Stratmann, R. E.; Yazyev, O.; Austin, A. J.; Cammi, R.; Pomelli, C.; Ochterski, J. W.; Ayala, P. Y.; Morokuma, K.; Voth, G. A.; Salvador, P.; Dannenberg, J. J.; Zakrzewski, V. G.; Dapprich, S.; Daniels, A. D.; Strain, M. C.; Farkas, O.; Malick, D. K.; Rabuck, A. D.; Raghavachari, K.; Foresman, J. B.; Ortiz, J. V.; Cui, Q.; Baboul, A. G.; Clifford, S.; Cioslowski, J.; Stefanov, B. B.; Liu, G.; Liashenko, A.; Piskorz, P.; Komaromi, I.; Martin, R. L.; Fox, D. J.; Keith, T.; Al-Laham, M. A.; Peng, C. Y.; Nanayakkara, A.; Challacombe, M.; Gill, P. M. W.; Johnson, B.; Chen, W.; Wong, M. W.; Gonzalez, C.; Pople, J. A. *Gaussian 03*, revsion B.05, Gaussian Inc.: Pittsburgh, PA, 2003.

(35) Wilson, E. B.; Decius, J. C.; Cross, P. C. *Molecular Vibrations: The Theory of Infrared and Raman Vibrational Spectra*; McGraw-Hill: New York, 1955.

(36) McIntosh, D. F.; Peterson, M. R. General Vibrational Analysis Programs. *Quant. Chem. Prog. Exch. Bull.* **1989**, *9*(3); http://qcpe@indiana.edu

(37) McIntosh, D. F. *Theor. Chem. Acc.* **2010**, *125*, 177–184.

(38) Huang, K.; Rhys, A. *Proc. Roy. Soc. London* **1950**, *204A*, 406–423.

(39) Denning., R G. *Struct. Bonding (Berlin)* **1992**, *79*, 215–276.

(40) (a) Réal, F.; Vallet, V.; Marian, C.; Wahlgren, U. *J. Chem. Phys.* **2007**, *127*, 214302. (b) Réal, F.; Gomes, A. S. P.; Visscher, L.; Vallet, V.; Eliav, E. *J. Phys. Chem. A.* **2009**, *113*, 12504–12511.

(41) Wang, Q.; Pitzer., R. M. *J. Phys. Chem. A* **2001**, *105*, 8370–8375.

(42) (a) Li, J.; Bursten, B. E.; Liang, B.; Andrews, L. *Science* **2002**, *295*, 2242–2245. (b) Andrews, L.; Liang, B.; Li, J.; Bursten, B. E. *Angew. Chem., Int. Ed.* **2000**, *39*, 4565–4567.

(43) Li, J.; Bursten, B. E.; Andrews, L.; Marsden, C. J. *J. Am. Chem. Soc.* **2004**, *126*, 3424–3425.

(44) Andrews, L.; Liang, B.; Li, J; Bursten, B. E. *J. Am. Chem. Soc.* **2003**, *125*, 3126–3139.

(45) Infante, I.; Andrews, L.; Wang, X.; Gagliardi., L. *Chem.—Eur. J.* **2010**, *16*, 12804–12807.

(46) Infante, I.; Kovacs, A.; La Macchia, G.; Shahi, A. R. M.; Gibson, J. K.; Gagliardi, L. *J. Phys. Chem. A* **2010**, *114*, 6007–6015.

(47) (a) Griffiths, D. J. *Introduction to Quantum Mechanics*, 2nd ed; Pearson Education: Upper Saddle River, NJ, 2005; p 356−357. (b) McHale, J. L. *Molecular Spectroscopy*; Prentice Hall: Upper Saddle River, NJ, 1999; p108−109.